Chemosphere 199 (2018) 351–360

Contents lists available at ScienceDirect

Chemosphere

journal homepage: www.elsevier.com/locate/chemosphere

Effect of U(VI) aqueous speciation on the binding of uranium by the cell surface of *Rhodotorula mucilaginosa*, a natural yeast isolate from bentonites

Margarita Lopez-Fernandez [a, *, 1], Maria Romero-González [b], Alix Günther [c], Pier L. Solari [d], Mohamed L. Merroun [a]

[a] Department of Microbiology, University of Granada, Granada, Spain
[b] Department of Geography, The University of Sheffield, Sheffield, United Kingdom
[c] Institute of Resource Ecology, Helmholtz-Zentrum Dresden-Rossendorf, Dresden, Germany
[d] MARS Beamline, Synchrotron SOLEIL, L'Orme des Merisiers, Saint-Aubin, Gif-sur-Yvette Cedex, France

HIGHLIGHTS

- *Rhodotorula mucilaginosa* BII-R8 cells are involved in the biosorption of uranium.
- Yeast cells bind mobile uranium species from solution via a time-dependent process.
- Carboxyl groups at the cell surface attract U-hydroxides and U-hydroxo-carbonates.
- Formed uranium species interact with organic phosphate groups at the cell wall.
- Uranium complexes have a similar local coordination to that of meta-autunite.

GRAPHICAL ABSTRACT

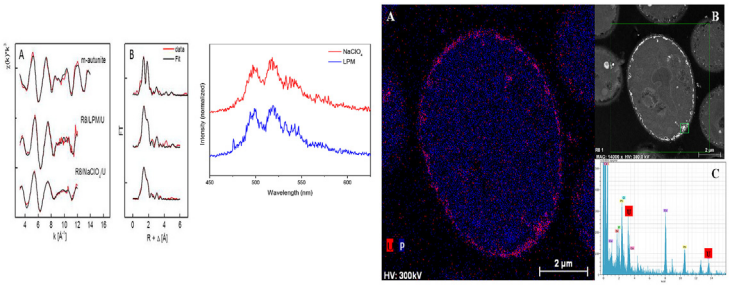

ARTICLE INFO

Article history:
Received 10 December 2017
Received in revised form
6 February 2018
Accepted 8 February 2018
Available online 9 February 2018

Handling Editor: Martine Leermakers

Keywords:
Uranium biosorption
Cell surface
Speciation

ABSTRACT

This study presents the effect of aqueous uranium speciation (U-hydroxides and U-hydroxo-carbonates) on the interaction of this radionuclide with the cells of the yeast *Rhodotorula mucigilanosa* BII-R8. This strain was isolated from Spanish bentonites considered as reference materials for the engineered barrier components of the future deep geological repository of radioactive waste. X-ray absorption and infrared spectroscopy showed that the aqueous uranium speciation has no effect on the uranium binding process by this yeast strain. The cells bind mobile uranium species (U-hydroxides and U-hydroxo-carbonates) from solution via a time-dependent process initiated by the adsorption of uranium species to carboxyl groups. This leads to the subsequent involvement of organic phosphate groups forming uranium complexes with a local coordination similar to that of the uranyl mineral phase meta-autunite. Scanning transmission electron microscopy with high angle annular dark field analysis showed uranium accumulations at the cell surface associated with phosphorus containing ligands. Moreover, the effect of uranium mobile species on the cell viability and metabolic activity was examined by means of flow

* Corresponding author. Centre for Ecology and Evolution in Microbial model Systems (EEMiS), Department of Biology and Environmental Science, Linnaeus University, Barlastgatan 11, 392 31 Kalmar, Sweden.
E-mail address: margarita.lopezfernandez@lnu.se (M. Lopez-Fernandez).
[1] Present address: Center for Ecology and Evolution in Microbial Model Systems (EEMiS), Linnaeus University, Kalmar, Sweden.

https://doi.org/10.1016/j.chemosphere.2018.02.055

Yeast *Rhodotorula*
Spectroscopy
Microscopy

cytometry techniques, revealing that the cell metabolism is more affected by higher concentrations of uranium than the cell viability.

The results obtained in this work provide new insights on the interaction of uranium with bentonite natural yeast from genus *Rhodotorula* under deep geological repository relevant conditions.

1. Introduction

The large amounts of radioactive waste generated by human activities (such as uranium mining and processing of the ores for the nuclear energy industry) will be disposed in future deep geological repositories (IAEA, 2003; SKB, 1999). This waste will be encapsulated into iron or copper canisters, surrounded by an engineered barrier consisting of bentonite, and embedded in the host rock (Alonso et al., 2008). The high microbial diversity of clay engineered barriers (Lopez-Fernandez et al., 2015; Poulain et al., 2008) could have an important impact on this barrier system through different processes such as corrosion of metal canisters (Stroes-Gascoyne et al., 2011); transformation of clay minerals (Pentráková et al., 2013); and radionuclide migration from the repository (due to biosorption (Morcillo et al., 2014), biotransformations (Martinez et al., 2014), biomineralization (Merroun et al., 2011), and intracellular accumulation (Brookshaw et al., 2012)). These activities may affect the safety of the repository by compromising its isolation.

The effects of microbial activity, cell structures and uranium binding ligands on the mobility of radionuclides depend on several parameters including the microbial species, the physical state of the microorganisms (planktonic or within biofilm) and metal aqueous speciation which depends on environmental parameters like O_2 and pH (Pedersen, 2002). Under oxic and acidic conditions (pH < 3) uranium occurs as uranyl ion, which is the most soluble, toxic and bioavailable form of uranium (Burns, 1999). However, under neutral and alkaline conditions, the uranium speciation is dominated by U hydroxides, U hydroxo-carbonates and U carbonates (Burns, 1999). Understanding the microbial interactions with radionuclides reveals the impact of microbial processes in the mobilization or immobilization of radionuclides. The interaction of uranyl ions with bacterial strains isolated from different environments including uranium contaminated sites (Cardenas et al., 2008; Dhal and Sar, 2014; Gerber et al., 2016; Kumar et al., 2013; North et al., 2004; Sánchez-Castro et al., 2017) and clay considered as host rock for deep geological disposal of radioactive wastes (Lopez-Fernandez et al., 2014; Lütke et al., 2013; Moll et al., 2015) have been widely studied. However, in the case of yeasts, although its distribution is widespread in the environment (Yurkov, 2017), most studies have been focused on the representative of phylum Ascomycota *Saccharomyces cerevisiae* (Lu et al., 2013; Wang et al., 2017; Zheng et al., 2017). Two recent studies demonstrated the ability of members of this phylum to bioprecipitate uranium as crystalline meta-autunite minerals (Liang et al., 2015) and the uranium uptake capacity by clay-fungal biomass (Olivelli et al., 2017). There are some studies describing interactions between Basidiomycota phylum members and uranium (Bai et al., 2012; Fomina et al., 2008; Liang et al., 2016). For instance, Bai et al. (2014) reported the uranium binding capacity of Ca-alginate mobilized cells of *Rhodotorula glutinis*. Nevertheless, no studies examined the effect of uranium aqueous speciation on the interaction of this radionuclide with species of the genus *Rhodotorula*. In this work we describe the molecular characterization of the interaction mechanisms of the strain *Rhodotorula mucilaginosa* BII-R8 with U hydroxides and U-hydroxo-carbonates under relevant conditions to that of the deep geological repository of nuclear wastes. The strain BII-R8 was isolated from bentonite clay deposits from Almeria, Spain (Lopez-Fernandez et al., 2014). These geological formations have been studied as analogue for the engineering barrier of the radioactive waste disposal system. Yeast species belonging to the genus *Rhodotorula* have been documented for their high heavy metal (Pb, Cd, Ag) and radionuclide tolerance, as well as binding capacity (Cho et al., 2011; de Silóniz et al., 2002; Li et al., 2008). Therefore, the objectives of this work are: 1) to investigate the effect of U aqueous species on the structure and local coordination of uranium within the cells of the strain BII-R8 by means of X-ray Absorption Spectroscopy (XAS), Time-Resolved Laser-induced Fluorescence Spectroscopy (TRLFS) and Fourier Transform Infra-Red (FT-IR) spectroscopy; as well as 2) to determine how the cells of *Rhodotorula mucilaginosa* BII-R8 tolerate the toxicity of uranium mobile species using Scanning Transmission Electron Microscopy-High Angle Annular Dark-Field (STEM-HAADF) and flow cytometry techniques.

2. Material and methods

2.1. Microbial cultures and uranium(VI) solution

The microbial cells were grown in LB medium consisting of 1.0 g/l tryptone, 0.5 g/l yeast extract, and 0.5 g/l NaCl at 28 °C on agitation (120 rpm). The pH of the medium was adjusted to 7. Low Phosphate Medium (LPM) (Table S1) and 0.1 M $NaClO_4$ were used as background electrolytes for the different uranium interaction experiments. 1 M stock solution of $UO_2(NO_3)_2 \cdot 6H_2O$ was prepared by dissolving the appropriate quantity of metal salt in 0.1 M $NaClO_4$. The stock solution was sterilized by filtration through 0.22 μm nitrocellulose filters and stored at 4 °C until use. Working solutions were prepared by dilution of the stock solution. The chemical speciation of U(VI) in LPM and in 0.1 M $NaClO_4$, at pH 7 and 25 °C was determined by using Visual Minteq 3.0 software (Gustafsson et al., 2009).

2.2. Sample preparation and experimental setup

2.2.1. TRLFS analyses

For TRLFS measurements, cells of *R. mucilaginosa* BII-R8 were incubated in triplicate with 1 mM U(VI) for 48 h in LPM and in 0.1 M $NaClO_4$, pH 7. After incubation, the cells were washed and suspended in 0.1 M $NaClO_4$, pH 7. The cells were harvested by centrifugation, dried under vacuum and subsequently powdered. All the measurements were performed in the Institute of Resource Ecology at the Helmholtz-Zentrum Dresden-Rossendorf in Germany. The samples were put on a special sample holder and were positioned in the laser beam. U(VI) luminescence at 25 °C was excited using a Nd-YAG laser (Minilite high-energy solid-state laser, Continuum) with laser pulses at 266 nm and an average pulse energy of about 250 μJ. The emissions were detected using an iHR 550 spectrograph and an ICCD camera. The luminescence spectra were recorded from 370 to 670 nm by accumulating 100 laser pulses using a gate time of

2 μs (complete detection system: HORIBA Jobin Yvon GmbH, Darmstadt, Germany). For time-resolved measurements a digital delay generator (DG535, Stanford Research Systems, Sunnyvale, CA, USA) was used. Subsequently, 51 U(VI) luminescence spectra were recorded at delay times between 0.05 and 50.05 μs with step sizes of 1 μs. Computer control over the entire system was ensured by the software Labspec 5 (HORIBA Jobin Yvon, Edison, New York, USA). The obtained luminescence data were processed by using Origin 7.5 (Origin Lab Corporation, Northampton, MA, USA) including peak fitting module. More equipment details are given in the handbook of applied solid state spectroscopy (Geipel, 2006).

2.2.2. XAS analyses

The cells of *R. mucilaginosa* BII-R8 were incubated with 1 mM U(VI) for 48 h in LPM and in 0.1 M $NaClO_4$, pH 7. After that, samples for XAS studies were prepared as previously described in Merroun et al. (2005). Briefly, cells were harvested and washed with 0.1 M $NaClO_4$. The pellets were dried in an oven at 30 °C for 24 h and subsequently powdered. Uranium L_{III}–edge X-ray absorption spectra were collected at the MARS beamline at the SOLEIL synchrotron facility (ring operated at 2.75 GeV with 400 mA), which is the French bending magnet beamline dedicated to the study of radioactive materials (Sitaud et al., 2012) using a Si(220) double-crystal monochromator with horizontal dynamical focusing, and Pt-coated mirrors for vertical focusing and rejection of higher harmonics (Solari et al., 2009). Spectra were collected in fluorescence mode using a 13-element Ge detector (EG & G ORTEC, USA). Data were processed and analyzed by using the ATHENA/ARTEMIS codes (Ravel and Newville, 2005). Background removal was performed by means of a pre-edge linear function. Atomic absorption was simulated with a square-spline function. The theoretical phase and amplitude functions used in data analysis were calculated with FEFF8 (Ankudinov et al., 1998) using the crystal structure of meta-autunite, $Ca(UO_2)_2(PO_4)_2 \cdot 6H_2O$ (Makarov and Ivanov, 1960) as a model.

All fits included the four-legged multiple scattering (MS) path of the uranyl group, U-Oax-U-Oax. The coordination number (N) of this MS path was linked to N of the single-scattering (SS) path U-Oax. The radial distance (R) and Debye-Waller factor (σ^2) of the MS path were linked at twice the R and σ^2 of the SS path U-Oax, respectively (Hudson et al., 1996). During the fitting procedure, N of the U-Oax SS path was held constant at two. The amplitude reduction factor (S_0^2) was held constant at 1.0 for the FEFF8 calculation and Extended X-Ray Absorption Fine Structure (EXAFS) fits. The shift in threshold energy, ΔE_0, was varied as a global parameter in the fits.

2.2.3. FT-IR analyses

R. mucilaginosa BII-R8 cells were harvested by centrifuging at 15000 × g for 15 min at 4 °C in an Eppendorf 5804R refrigerated centrifuge. Then, the biomass pellet was lyophilized using an Alpha 1–2 LD Plus freeze dryer. Samples for the analyses were prepared by adding 0.1 g of dry biomass to different uranium solutions ranging from 0.01 to 1 mM U(IV) prepared in 0.1 M $NaClO_4$. The pH was adjusted to 7 and incubation was performed in triplicate at 28 °C on agitation at 120 rpm for 2, 8, 24, 32 and 48 h. Measurements were performed using Attenuated Total Reflectance (ATR)-FT-IR with an angle of incidence of $\theta = 45$ at 4 cm^{-1} spectral resolution. Measurements were obtained using a Silver Gate Evolution ATR accessory, consisting of a germanium crystal, coupled to a Perkin Elmer Spectrum One FT-IR spectrometer. A total of 30 scans were performed on each sample within the scanning range 2000–800 cm^{-1}. An average spectrum was obtained from 3 replicates and normalized. All data acquisition and processing were performed using the PerkinElmer Spectrum version 3.3.

2.2.4. STEM-HAADF and EDX analyses

R. mucilaginosa BII-R8 cells were incubated with 1 mM U(VI) for 48 h in LPM, pH 7. After the incubation, uranium treated cells were harvested by centrifugation at 15000 × g for 15 min at 4 °C and washed twice with 0.9% NaCl to remove the interfering ingredients of the growth medium. TEM samples were prepared as described in Merroun et al. (2005). Samples were examined by using a STEM-HAADF FEI TITAN G2 80–300. TEM specimen holders were cleaned by plasma prior to STEM analysis to minimize contamination. The high resolution STEM is equipped with a HAADF detector and an EDX energy dispersive X-ray detection system.

2.2.5. Flow cytometry analyses

R. mucilaginosa BII-R8 cell cultures were prepared in triplicate and loaded for 24/48 h with two different uranium concentrations (0.5 and 1 mM U). Cells were harvested from LPM medium, by centrifugation (15000 × g, 15 min, 4 °C), suspended and diluted in Phosphate Buffered Saline (PBS) to adjust the cell concentration to the required one for this experiment (approximately 10^6 cells/ml). *R. mucilaginosa* BII-R8 cells were incubated in triplicate and harvested under the same conditions but without uranium, as control. For live dead/staining, solutions of Fluorescein Di-Acetate (FDA) (Acros Organics) (20 μl, 0.1 mg/ml) and Propidium Iodide (PI) (2 μl, at 1 mg/ml) (Invitrogen) were mixed with cell suspensions for 15 min in dark, at room temperature. Cell suspensions incubated in the presence of both stains simultaneously were analyzed by flow cytometry for green (i.e. viable) and red (i.e. dead). To study the effect of U(VI) on the cell metabolic activity, a PBS-suspension of approximately 10^6 cells/ml of the harvested cells were incubated with 20 μl of 10 μM $DiOC_6$ (Invitrogen) in dark for 15 min at room temperature. Measurements were taken in triplicate using a FACSCantoII cytometer Becton Dickinson (San Jose Palo Alto, California), equipped with three lasers: 488 nm blue, 620 nm red and 405 nm UV. Samples were measured in FL1 (FDA-FITC) and FL2 (PI-PE), in logarithmic scale channels, at medium speed. The filters used for the measurements were 530 nm and 580 nm band pass. Samples were analyzed using BD Diva 6.1.

3. Results

3.1. Chemical speciation of uranium in LPM and $NaClO_4$

The chemical speciation of U(VI) in the presence of 0.1 M $NaClO_4$ and LPM at different metal concentrations (in the absence of microbial cells) is shown in Table 1. In the experiment using 0.1 M $NaClO_4$, at 0.5 and 1 mM U concentration (pH 7), the uranium speciation is dominated by hydroxo-uranyl complexes. In both cases, the uranium speciation is controlled by $(UO_2)_3(OH)_5^+$ (54.9 and 50.0%) and $(UO_2)_4(OH)_7^+$ (44.5 and 49.6%), at 0.5 and 1 mM U, respectively. In contrast, in LPM at uranium concentrations of 0.5 mM and 1 mM, the speciation of U(VI) is dominated by uranyl hydroxo-carbonates ($(UO_2)_2CO_3(OH)_3^-$). The minor uranium species are $(UO_2)_3(OH)_5^+$, represented by 9.1 and 11.7% and $(UO_2)_4(OH)_7^+$

Table 1
Calculated aqueous speciation of uranium in LPM and $NaClO_4$ 0.1 M, before adding cells.

Uranium species	U(VI) concentration (mM)			
	0.5		1	
	LPM	$NaClO_4$	LPM	$NaClO_4$
$(UO_2)_2CO_3(OH)_3^-$	85.7%	–	80.0%	–
$(UO_2)_3(OH)_5^+$	9.1%	54.9%	11.7%	50.0%
$(UO_2)_4(OH)_7^+$	4.5%	44.5%	7.8%	49.6%

with values of 4.5 and 7.8%, at 0.5 mM and 1 mM of U concentrations, respectively.

3.2. TRLFS analyses of U-complexes formed by the cells of the yeast *R. mucilaginosa* BII-R8

The luminescence spectra recorded by TRLFS from *R. mucilaginosa* BII-R8 cells, incubated with 1 mM U(VI) at pH 7 in 0.1 M $NaClO_4$ and LPM solution, are shown in Fig. 1 and the corresponding luminescence emission maxima are summarized in Table 2. Three main emission fluorescence bands were detected in $NaClO_4$ (498.4, 517.7 and 540.0 nm) and LPM (497.9, 518.1 and 538.9 nm). Comparing these determined parameters to those of reference compounds, the luminescence properties of the cells incubated at pH 7 are characteristic of U(VI) complexes formed with phosphate groups of organic molecules such as sugar phosphates including fructose phosphates (Koban et al., 2004), phosphorylated nucleosides (e.g. AMP) (Merroun et al., 2003b), or lipopolysaccharides of the gram-negative bacterium *E. coli* (Barkleit et al., 2008). These results indicate that mainly organic phosphate residues of the yeast cells are responsible for the complexation of U(VI). The similar location of the emission bands of organic uranyl carboxylate complexes (Table 2) indicates that carboxyl groups are also involved in the uranium complexation. The analysis of the time-resolved measurements showed a bi-exponential uranyl luminescence decay for both samples (not shown here). That means, two different uranyl species in each sample were formed with luminescence lifetimes of 1.8 and 11.1 μs for the samples incubated in $NaClO_4$ and 2.2 and 11.3 μs for the LPM-incubated samples, both at pH 7. They are highly comparable to each other (Table 2). However, it is not possible to assign the determined lifetimes to defined solid uranyl species because there is not enough model data of different organic uranyl phosphates. Fitting procedures at different delay times showed no shift of the luminescence emission maxima, indicating a high structural similarity of the formed complexes.

3.3. XAS analyses

The L_{III}-edge EXAFS spectra of the species formed by the yeast cells at 1 mM metal concentration and their corresponding Fourier Transforms (FT) are presented in Fig. 2. The FT represents a pseudo-radial distribution function of the uranium near-neighbor environment. The FT peaks appear at lower *R*-values (R + Δ) relative to the true near-neighbor distances R as a result of the EXAFS phase shift. This shift depends on the scattering phase function ϕ of the electron wave and originate a shift in the interatomic distance of Δk = 0.2–0.5 Å.

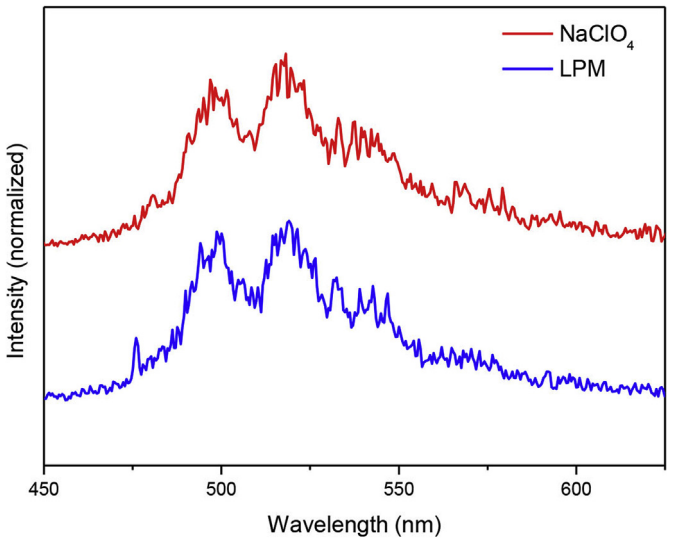

Fig. 1. Luminescence spectra obtained with an excitation wavelength of 410 nm of the U(VI) complexes formed by the yeast cells *R. mucilaginosa* BII-R8 after 48 h incubation with 1 mM U at neutral pH, in 0.1 M $NaClO_4$ and in LPM.

The uranyl unit consists of a uranium center with a formal charge of +6 coordinated to two double-bonded oxygen atoms to form a *trans*-dioxo cation, UO_2^{2+}. This "axial" unit is highly stable and binds to other ligands via the formation of U–O bonds in a plane perpendicular to the axis of the uranyl ion. The "equatorial" oxygen (O_{eq}) coordination number varies from 4 to 6 depending on the chemical environment, and these equatorial bonds are the sole means of complexation available for uranyl units under normal conditions. Standard compounds used for comparison were inorganic uranyl phosphate (m-autunite). The FT of the EXAFS spectra of two samples, in LPM and in 0.1 M $NaClO_4$ show six significant peaks (Fig. 2). The EXAFS spectra of the two samples present high similarity indicating that the local coordination of U(VI) within the two samples is similar. Quantitative fit results (Table 3) (distances are phase shift corrected) indicate that the adsorbed U(VI) has the common linear *trans*-dioxo structure: two axial oxygen atoms at about 1.78–1.79 ± 0.02 Å, and an equatorial shell of 4 oxygen atoms at 2.27–2.28 ± 0.02 Å. As evident from the results presented in Table 3, the Debye-Waller factors of the U–O_{eq1} shell is affected by the background electrolyte (LPM and $NaClO_4$). In the EXAFS spectra of the samples in LPM, we observed a fourth-fold coordination of uranium to ligands of the bacterial cells (N ~ 4 and R = 2.28 ± 0.02 Å). The lower Debye-Waller factor (0.0063 $Å^2$) implies the absence of a disorder in U–O_{eq1} distances contributing to the EXAFS. However, the higher Debye-Waller factor of the EXAFS spectrum of $NaClO_4$ (0.011 $Å^2$) indicated that there is probably a wide spread of U–O_{eq1} distances with an averaged value of 2.27 ± 0.02 Å. The U-Oeq_1 bond distance in the two samples is within the range of previously reported values for the oxygen atom of the phosphate bound to uranyl (Merroun et al., 2003a, 2011; Nedelkova et al., 2007).

In all samples, the addition of a shell of one oxygen scatter at distance of R = 2.86–2.87 ± 0.02 Å improve significantly the fit. Such a distance between uranium and oxygen atoms is not related to direct bonding but they are interpreted in several systems as scattering contributions from neighboring ligand shells known as "short contacts" in crystallography (Jroundi et al., 2007; Merroun et al., 2003a; Nedelkova et al., 2007). The fifth FT peak, which appears at R+Δ ~3 Å (radial distance R = 3.58 Å) is a result of the backscattering from phosphorus atoms. This distance is typical for a monodentate coordination of U(VI) by phosphate. The EXAFS spectra of the U-treated yeast cell samples in LPM and $NaClO_4$ are similar to that of m-autunite with regard to the U-Oeq, U–P distances, suggesting that an inorganic m-autunite-like uranyl phosphate phase was precipitated by the yeast cells in these two samples.

3.4. FT-IR results

FT-IR spectra were collected in order to identify changes in chemical surface compounds of *R. mucilaginosa* BII-R8. The interactions between *R. mucilaginosa* and uranium that can be observed using this technique are mainly surface interactions. Fig. 3 shows a summary of the results obtained from the kinetics and sorption of uranium (Fig. 3a) and the dependency on uranium concentration (Fig. 3b) studies. No major changes were observed on the spectral region at 1640 cm^{-1}, hence this band was used to

Table 2
Luminescence emission maxima of the U(VI) complexes formed by *R. mucilaginosa* BII-R8 cells in LPM and $NaClO_4$ at 1 mM U and selected uranyl model complexes.

	Main luminescence emission bands (nm)			Lifetimes (μs)		Reference
Samples						
R. mucilaginosa-$NaClO_4$	498.4	517.7	540.0	1.8 ± 0.1	11.1 ± 0.3	This work
R. mucilaginosa-LPM	497.9	518.1	538.9	2.2 ± 0.1	11.3 ± 0.4	This work
Reference samples						
Organic uranyl phosphate complexes						
UO_2-fructose(6) phosphate	497.1	519.0	543.3	0.13 ± 0.05		Koban et al., 2004
UO_2-AMP	497	519	542	n.d.		Merroun et al., 2003b
R-O−PO_3−UO_2	498.1	519.6	542.9	1.2 ± 0.4		Barkleit et al., 2008
Inorganic uranyl phosphate complexes						
$UO_2PO_4^-$	502	524	548	n.d.		Bonhoure et al., 2007
$(UO_2)_x(PO_4)_y$	503.0	523.7	546.9	n.d.		Brendler et al., 1996
Organic uranyl carboxylate complexes						
Uranyl acetate	494.6	514.3	535.9	23.7 ± 1.3	23.0 ± 2.4	Reitz et al., 2015
R−COO−UO_2^+/(R−COO)$_2$-UO_2	498.1	518.0	539.0	0.7 ± 0.1		Reitz et al., 2015
UO_2^{2+} and hydrolytic species						
UO_2^{2+}aq. (pH 1, I = 0.1 M)	488.9	510.5	533.9	1.8 ± 0.2		Geipel et al., 2000
UO_2OH^+	498	519	543	35 ± 2		Brachmann et al., 2002
$(UO_2)_2(OH)_2^{2+}$	499	519	542	2.9 ± 0.4		Kato et al., 1994
$(UO_2)_3(OH)_5^+$	496	514	535	23 ± 3		Moulin et al., 1998
Uranyl carbonate minerals						
$Ca_2[UO_2(CO_3)_3]\cdot 10H_2O$	482.9	502.7	524.5	145 ± 5		Amayri et al., 2005
$Ca_2(UO_2)(CO_3)_3\cdot 11H_2O$	483.1	502.7	524.1	313 ± 10		Amayri et al., 2005
$Ca_2[UO_2(CO_3)_3]$ in solute	484	504	524	0.04 ± 0.01		Bernhard et al., 2001
Uranyl phosphate minerals						
Autunite	504.0	524.2	548.0	5.15 ± 0.28		Geipel et al., 2000
Meta-autunite	501.8	522.9	546.9	0.74 ± 0.10		Geipel et al., 2000
$Mg[UO_2PO_4]_2\cdot 10H_2O$	501.1	522.1	545.7	2.25 ± 0.20		Geipel et al., 2000

Error of emission bands is ±0.5 nm.

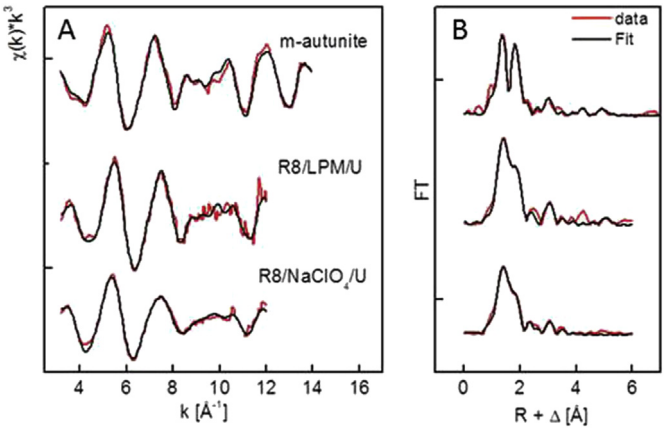

Fig. 2. A) Uranium L_{III}-edge k^3–weighted EXAFS spectra and B) the corresponding Fourier transforms (FT) of the uranium complexes formed by *R. mucilaginosa* BII-R8 cells at U concentrations of 1 mM in LPM and $NaClO_4$, and reference compound (m-autunite).

Table 3
Structural parameters of the uranium complexes formed by the cells of the strain *R. mucilaginosa* BII-R8 in 1 mM U using both LPM and $NaClO_4$ as background electrolyte. Meta-autunite structural parameters were included as comparison.

Sample	Shell	N[a]	R(Å)[b]	σ^2 (Å^2)[c]	ΔE (eV)
LPM	U-O_{ax}	2[d]	1.78	0.0039	0.56
	U-O_{eq1}	4.2(4)	2.28	0.0063	
	U− O_{eq2}	0.8(2)	2.86	0.0038[d]	
	U−P	3.3(4)	3.58	0.004	
	U− O_{eq1}-P (MS)	6.6[e]	3.68[f]	0.004	
$NaClO_4$	U-O_{ax}	2[d]	1.79	0.0069	−0.2
	U-O_{eq1}	4.5(3)	2.27	0.011	
	U− O_{eq2}	1.0(2)	2.87	0.0038[d]	
	U−P	3.2(5)	3.58	0.0040	
	U− O_{eq1}-P (MS)	6.4[e]	3.69[f]	0.0040	
m-autunite	U-O_{ax}	2[d]	1.77	0.0025	−13.40
	U-O_{eq1}	4.8(5)	2.34	0.0105	
	U− O_{eq2}	0.8(2)	2.86	0.0038[d]	
	U−P	1.5(3)	3.60	0.0010	
	U− O_{eq1}-P (MS)	3.0[e]	3.73[f]	0.0010	

[a] Errors in coordination numbers are ±25%, and standard deviations, as estimated by EXAFSPAK, are given in parentheses.
[b] Errors in distance are ±0.02 Å.
[c] Debye-Waller factor.
[d] Value fixed for calculation.
[e] Coordination numbers for U−P and U-Oeq1-P were linked.
[f] Debye Waller factors for U−P and U-Oeq1-P were linked.

normalise all spectrum. The spectra of *R. mucilaginosa* BII-R8 used as control exhibited a composition typical for microbial cells. The band at 1640 cm^{-1} is accompanied by a band at 1543 cm^{-1} that has been assigned to the stretching of the conjugated double bond of the carbonyl, C=O, group from amides (Barth, 2007). The presence of this group corresponds to proteins of the yeast membrane. The spectra also display absorption bands between 1050 and 1150 cm^{-1} and 1070–1150 cm^{-1}, which have been assigned to C−O stretching modes (Galichet et al., 2001) indicating the presence of alcohol and ether groups, respectively. Interestingly, the band at 917 cm^{-1}, assigned to the stretching of U=O (Romero-Gonzalez et al., 2016), is absent in the *R. mucilaginosa* BII-R8 control spectrum (Fig. 3a). At longer contact times, the shape of the band changes, from broad to sharp. The presence of this band has been assigned to the stretching of U=O that has shifted from 938 cm^{-1} compared to the control $UO_2(NO_3)_2$ spectrum and the changes are associated to the accumulation of UO_2^{2+} on the surface of *R. mucilaginosa* BII-R8. Moreover, the bands at 1240 and 1076 cm^{-1} are characteristic of vibrational asymmetric stretching of phosphate (Hufton et al., 2016). These groups are able to complex several metals within the cellular membrane or other yeast components such as peptides, phospholipids or peptidoglycan.

There is an interesting change evident on the band at 1390 cm^{-1} (Fig. 3a). This is a band characteristic to stretching of carboxylate anions (COO−) (Galichet et al., 2001), where the vibration may be affected by changes on the binding environment of the carboxylate

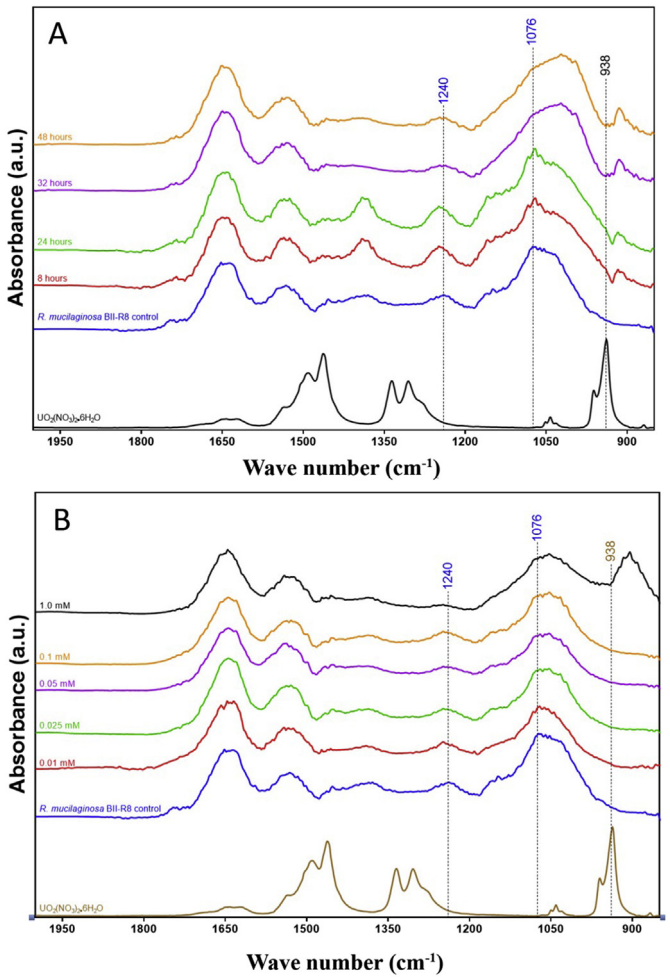

Fig. 3. 2000-800 cm^{-1} FTIR region of *R. mucilaginosa* BII-R8 cells after uranium binding as a function of A) time, concretely 8, 24, 32 and 48 h and B) uranium concentrations ranging from 0.01 to 1 mM U(VI).

group. The change of the intensity of vibration over time seems to indicate a change of composition of the carboxylate group, resulting on an increased intensity at 8 h and 24 h that is reduced to levels comparable to the *R. mucilaginosa* BII-R8 control over longer periods of time. This phenomenon was not observed on the sorption experiments, since the batch was conducted at 48 h (Fig. 3b).

3.5. STEM-HAADF and EDX analyses

STEM-HAADF micrographs of thin sections of *R. mucilaginosa* BII-R8 cells exposed to 1 mM U(VI) are shown in Fig. 4. In these micrographs, electron-dense precipitates were observed at the cell surface. In addition, intracellular U accumulations are localized within and at the membranes of concentric organelles. The EDX spectra of the accumulated uranium displayed X-ray emission peaks corresponding to U and P (Fig. 4c). The copper (Cu) peak resulted from the copper grid used to support the specimen and the presence of the silicon (Si) peak can be attributed to culture impurities.

3.6. Effect of U(VI) on cell viability and metabolic activity

To determine the ability of the cells of *R. mucilaginosa* BII-R8 to tolerate different uranium concentrations, LPM was used as oligotrophic culture medium where the cells could grow. Flow cytometry studies revealed that the cell viability depends on the U concentration and incubation time. After 24 h of incubation at different uranium concentrations the yeast *R. mucilaginosa* BII-R8 cells were abundantly alive (>90%) and not very affected by this radionuclide (Fig. 5a and Table S2). However, after 48 h of incubation time the cell viability of the yeast cells was decreased compared to that of 24 h (Fig. 5b). At 0.5 mM of uranium concentration, the viability was reduced from 96 to 92%. When the uranium concentration was increased to 1 mM, the viability dropped to 85%. The metabolic activity of *R. mucilaginosa* BII-R8 cells after 48 h of incubation was decreasing proportionally to the decrease of the cell viability (Fig. 6 and Table S3). These analyses showed that the metabolic activity of the yeast cells was affected at 1 mM of uranium concentration (decreasing to 74%). Therefore, the cell metabolism is much more affected by higher concentrations of uranium than the cell viability.

4. Discussion

The present work aimed to investigate the effect of aqueous uranium speciation on the uranium interactions with the yeast *Rhodotorula mucilaginosa,* isolated from Spanish bentonites. Two different geochemical conditions (GC) were simulated: the electrolyte $NaClO_4$ representative of typical ionic strength of groundwater (GC1) where the aqueous uranium speciation was dominated by positively charged U hydroxide species ($(UO_2)_3(OH)_5^+$ and $(UO_2)_4(OH)_7^+$); the GC2 corresponds to the LPM system where the aqueous uranium speciation was controlled by negatively charged U-hydroxo carbonates species $(UO)_2CO_3(OH)_3^-$.

TRLFS analysis showed that the main fluorescence emission bands of the uranium complexes formed under these two geochemical conditions are similar and demonstrated that uranium is bound preferably to organic phosphate ligands (Barkleit et al., 2008; Koban et al., 2004; Merroun et al., 2003b). The local coordination of U(VI) at the yeast cells was determined by XAS, revealing that the uranium is complexed by phosphoryl groups four-fould monodentate coordinated in the equatorial plane of the uranyl dioxo-cation, comparable to the uranyl mineral phase meta-autunite. These complexes were mainly localized at the cells surface, as demonstrated by the STEM.HAADF analysis.

These apparently contradictory results obtained by TRLFS and XAS showed that the *R. mucilaginosa* BII-R8 cells are involved in the biosorption of U-hydroxo-carbonates and U-hydroxides species and formation of U-organic phosphate complexes. However, the data presented in this work are in agreement with those previously reported by Barkleit et al. (2011) who also showed a discrepancy between XAS and TRLFS measurements. Similar to our work, the XAS analysis showed that the structural parameters of U(VI) complexes formed by purified lipopolysaccharide of *E. coli* were similar to that of meta-autunite, but in contrast their fluorescence parameters were comparable to those of U-phosphate group complexes and different to those of m-autunite. These results indicate that the speciation of uranium associated with the cells of *R. mucilaginosa* is not controlled by the aqueous uranium speciation but by functional groups reactive to the presence of uranium in the cell surface. The findings are contrasting with results reported by Kulkarni et al. (2013). In this study, the speciation of uranium (under low and high carbonate conditions) had an effect on the biosorption and bioprecipitation of uranium by *Deinococcus radiodurans* and *Escherichia coli*, despite their phosphatase activity. The authors attributed the low uranium biosorption capacity under high carbonate concentration conditions to the repulsion of the predominantly negatively charged aqueous uranium complexes by the bacterial cell surface. However, under low carbonate conditions

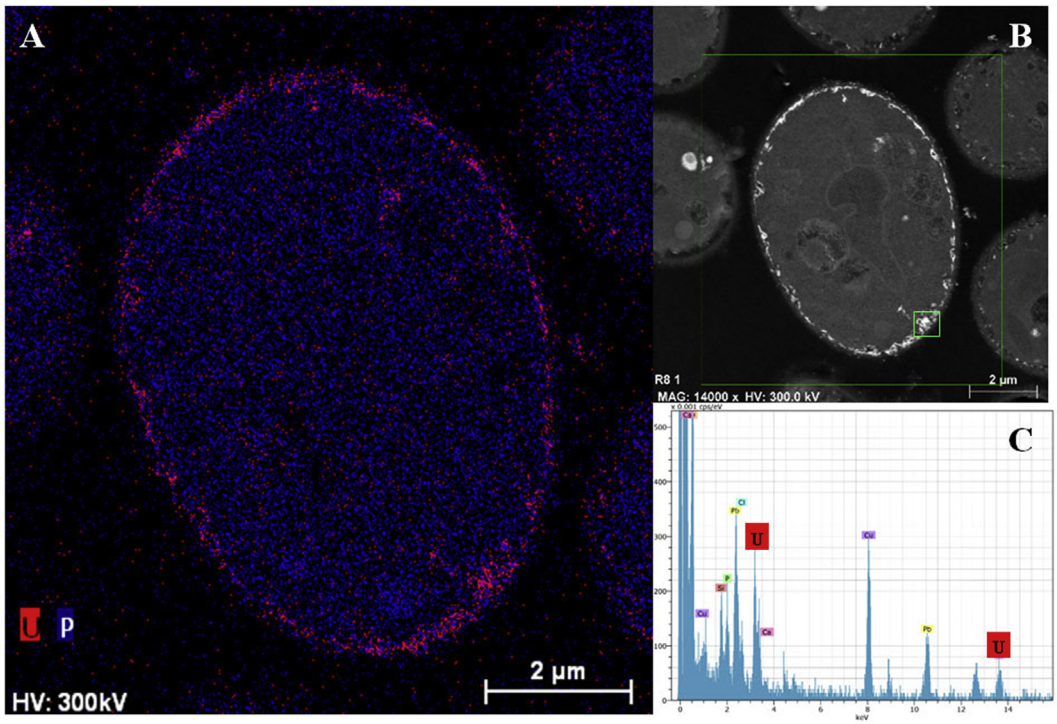

Fig. 4. Scanning Transmission Electron Microscopy-High-Angle Annular Dark-Field (STEM-HAADF) micrographs of thin sections of *R. mucilaginosa* BII-R8 treated with 1 mM U (A and B). Energy Dispersive X-ray spectrum of U complexes at the cell walls (C).

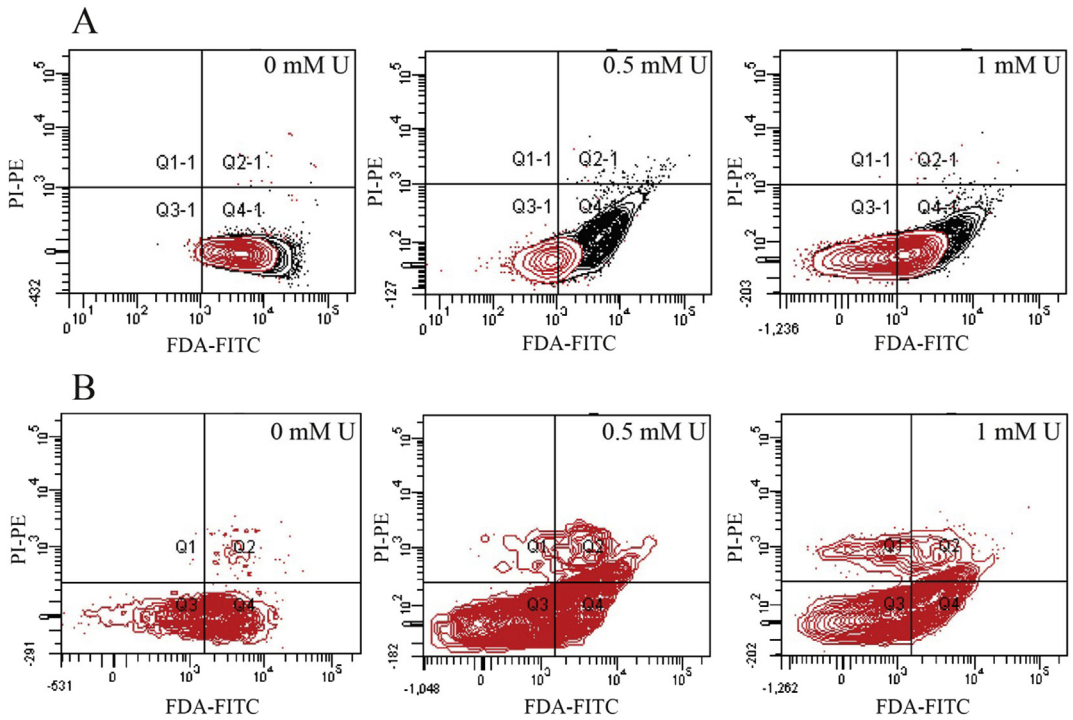

Fig. 5. Flow cytometry scatterplots of BII-R8 cell viability after A) 24 h at uranium concentration ranging from 0 to 1 mM. Q1-1: dead cells (PI+, FDA-), Q2-1: damaged cells, considered as dead cells (PI+, FDA+), Q3-1: cellular rest, not considered in this study (PI−, FDA-), Q4-1: alive cells (PI−, FDA+); and B) 48 h, at uranium concentration ranging from 0 to 1 mM. Q1: dead cells (PI+, FDA-), Q2: damaged cells, considered as dead cells (PI+, FDA+), Q3: cellular rest, not considered in this study (PI−, FDA-), Q4: alive cells (PI−, FDA+).

the predominant positively charged aqueous uranium species allow the uranium to interact with the cells.

FT-IR analyses were used to study the kinetics of U biosorption by the cells of the yeast strain under geochemical conditions dominated by positively charged U hydroxides (GC1). The interaction with uranium is a time-dependent process, where at shorter time, the U hydroxides species present initially are attracted to the negatively charged carboxyl groups at the cell surface. This leads to

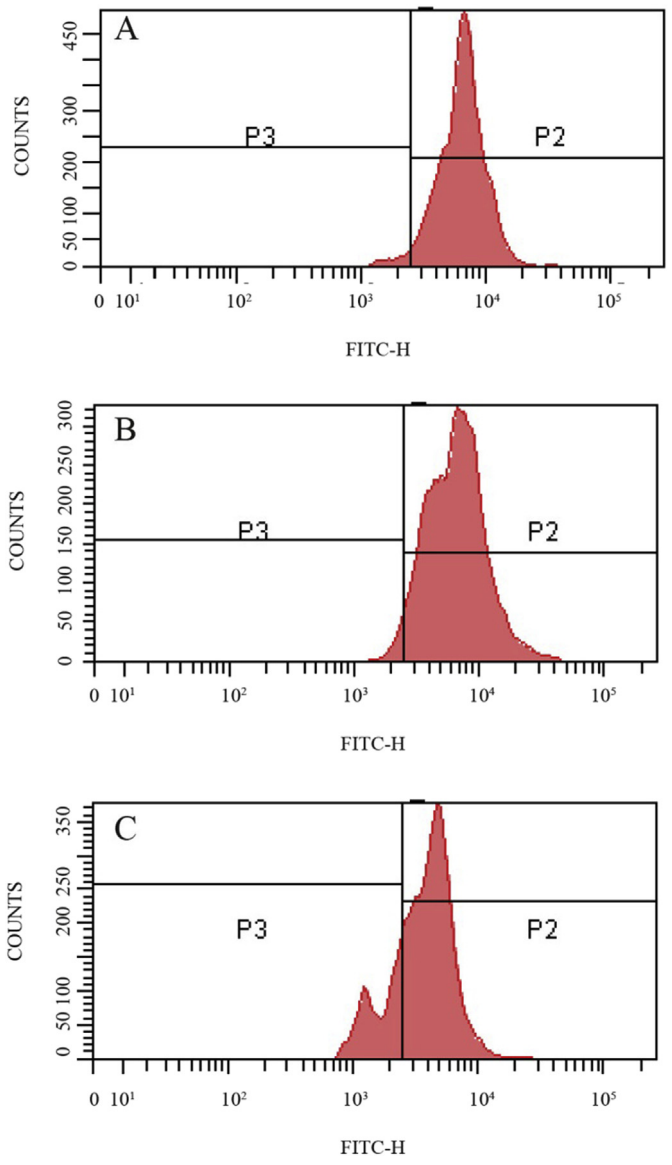

Fig. 6. Flow cytometry scatterplots of BII-R8 membrane potential after 48 h, at different uranium concentrations. A. 0 mM, B. 0.5 mM, C. 1 mM,. P2: metabolically active cells, P3: metabolically inactive cells.

the interaction of the formed U species with neighboring phosphate groups at longer time contact. This method revealed the involvement the carboxyl groups in the biosorption of uranium species against what the XAS in particular was not able to detect the contribution of the carboxylic ligands in the binding of uranium, probably due to their low concentration after the long incubation time of the samples studied (48 h).

STEM-HAADF and flow cytometry techniques were used to assess the toxicity of negatively charged uranium hydroxides species towards the cells of the yeast strain *R. mucilaginosa* BII-R8. Uranyl organic phosphate groups seem to play a major role in detoxification of U(VI) since STEM-HAADF analysis showed that uranium is accumulated mainly at the cell wall. Three main components form the yeast cell wall: glucan (up to 56%), mannoprotein (up to 50%) and chitin (approximately 6%), whereas only small and variable amounts of lipid have been reported (Aguilar-Uscanga and Francois, 2003; Villegas et al., 2009). The functional groups involved in the binding of U(VI) by the yeast are probably the carboxyl sites within the polysaccharides of the cell as well as the phosphoryl groups of the phospholipid bilayer of the cytoplasmic membrane.

Flow cytometry analysis showed that the cell viability is an incubation time-dependent process. The uranium tolerance of the yeast cells seems to be biologically mediated, due to the differences in the level of uranium tolerance among several microbial strains isolated from the same bentonite samples under the same experimental conditions (Lopez-Fernandez et al., 2014). In addition, the effect of uranium on the cell metabolic activity was also investigated using $DiOC_6$, a fluorescent lipophilic dye used for staining mitochondria in living yeast cells (Koning et al., 1993). These results revealed that after 48 h of incubation at 1 mM of uranium concentration, a high percentage of the cell metabolism (74%) was still active. The oxidative stress induced by the yeast cells at high uranium concentrations may result in the formation of reactive oxygen species (ROS) which highly damage cellular components, like DNA, lipids and proteins as previously described by Imlay (2003). To cope with the toxicity of these ROS, microorganisms have developed different strategies including reduction or precipitation of the dangerous component causing the ROS, ion exchange and reverse osmosis (Cheung and Gu, 2007). An example of yeast detoxification mechanisms against different heavy metals was described for *Schizosaccharomyces pombe* in Prévéral et al. (2009).

4.1. Implications for geological repositories

Microorganisms can contribute to the speciation of radionuclides and radionuclide mobility through the geosphere (Lloyd and Renshaw, 2005). Microbial activity also has an effect in the structural stability and performance of engineered barriers, including corrosion of canisters and deterioration of concrete through changes in porosity and biofilm formation (Masurat et al., 2010; Pedersen, 2010). In the case of Spanish bentonites, there is little information on the effect of existing microbial communities may have on the structure or performance of this material as an artificial barrier. This is one of the first studies describing the influence of strain *R. mucilaginosa* BII-R8 in the transport and mobility of radionuclides. It would therefore be expected that under environmental conditions, such as excavation, construction and installation, this microorganism can thrive and form an established community. This would ensure survival over time and may have an influence on bentonite structure and porosity. The yeast strain *R. mucilaginosa* BII-R8 showed abilities for retaining uranium from solution irrespective of its chemical specie. The mechanism of removal is varied, showing that this microorganism can adapt to different solution composition and radionuclide chemical speciation, which makes it reactive under a variety of environmental situations. This study shows that sorption and removal of uranium is favored in the presence of carbonates and the yeast strain *R. mucilaginosa* BII-R8 is capable to tolerate high concentrations of this radionuclide. This could represent an advantage in case of failure of geological repositories, where radionuclides can escape and be leached into the subsurface.

The results from this study demonstrated the value of research in analogue environments representative of repositories. We have provided evidence from molecular microbiology and biogeochemistry that the presence of microorganisms such as *Rhodotorula mucilaginosa* BII-R8 in bentonite clays is positive, providing the barrier with additional ability to retain radionuclides. Therefore, one obvious question to explore for advancing our ability to predict microbial dynamics in geological repositories is to what extent the presence of microorganisms may modify clay structure and stability.

5. Conclusions

The present study provide new molecular insights into the effect of aqueous uranium speciation in the interaction of uranium with natural microbes from bentonite formations considered as artificial barriers for the future deep geological repositories. This study was performed under relevant geochemical conditions for this kind of disposal systems where different uranium species could be present. The results showed that the uranium tolerance of the yeast cells is a time-dependent process. . In a first step, U-hydroxides and U-hydroxo-carbonates are attracted to the carboxyl groups at the cell surface, allowing in a second step its interaction with organic phosphate groups that finally accumulates at the cell wall. These data indicated that the U(VI)-yeast interaction makes this radionuclide less mobile, having a positive effect in the concept of the radioactive waste disposal. However, long-term studies should be performed to assess the stability of these uranium complexes, as well as to further characterize the microbial processes impact in the mobilization/immobilization of radionuclides in the deep geological disposal of radioactive wastes.

Author contributions

MLM conceived the study; ML-F carried out the sampling, prepare the samples and carried out the experiments; AG performed the TRLFS analysis, ML-F, PLS and MLM carried out the EXAFS measurements; MLM analyzed the EXAFS spectra; MR-G formulated and designed the FT-IR studies; ML-F, MR-G, AG, PLS and MLM interpreted data; ML-F and MLM drafted the manuscript that was approved by all authors.

Funding

This work was funded by Grants CGL2009-09760, BES-2010-032098, EEBB-I-12-04964 and CGL-2012-36505 (80% finding by FEDER) (Ministerio de Ciencia e Innovación, España).

Conflicts of interest

The authors declare no conflict of interest.

Acknowledgments

We acknowledge the assistance of María del Mar Abad Ortega, and Concepción Hernández-Castillo (Microscopy Service, Centro de Instrumentación Científica, University of Granada, Spain); of Jaime Lazuen-Alcon (Flow Cytometry Service, Centro de Instrumentación Científica University of Granada, Spain); of Björn Drobot for the Parafac calculations and Monika Dudek for microbiology support (HZDR, Germany); Ahinara Amador-Garcia and Ivan Sanchez-Castro (Department of Microbiology, University of Granada) for their help with the EXAFS measurements; and Joseph Hufton (University of Sheffield, UK) for the FT-IR art work.

Appendix A. Supplementary data

Supplementary data related to this article can be found at https://doi.org/10.1016/j.chemosphere.2018.02.055.

References

Aguilar-Uscanga, B., Francois, J., 2003. A study of the yeast cell wall composition and structure in response to growth conditions and mode of cultivation. Lett. Appl. Microbiol. 37, 268–274.

Alonso, E.E., Springman, S.M., Ng, C.W.W., 2008. Monitoring large-scale tests for nuclear waste disposal. Geotech. Geol. Eng. 26, 817–826.

Amayri, S., Reich, T., Arnold, T., Geipel, G., Bernhard, G., 2005. Spectroscopic characterization of alkaline earth uranyl carbonates. J. Solid State Chem. 178, 567–577.

Ankudinov, A., Ravel, B., Rehr, J., Conradson, S., 1998. Real-space multiple-scattering calculation and interpretation of x-ray-absorption near-edge structure. Phys. Rev. B 58, 7565.

Bai, J., Wu, X., Fan, F., Tian, W., Yin, X., Zhao, L., et al., 2012. Biosorption of uranium by magnetically modified Rhodotorula glutinis. Enzym. Microb. Technol. 51, 382–387.

Bai, J., Li, Z., Fan, F., Wu, X., Tian, W., Yin, X., et al., 2014. Biosorption of uranium by immobilized cells of Rhodotorula glutinis. J. Radioanal. Nucl. Chem. 299, 1517–1524.

Barkleit, A., Moll, H., Bernhard, G., 2008. Interaction of uranium (VI) with lipopolysaccharide. Dalton Trans. 2879–2886.

Barkleit, A., Foerstendorf, H., Li, B., Rossberg, A., Moll, H., Bernhard, G., 2011. Coordination of uranium (VI) with functional groups of bacterial lipopolysaccharide studied by EXAFS and FT-IR spectroscopy. Dalton Trans. 40, 9868–9876.

Barth, A., 2007. Infrared spectroscopy of proteins. Biochim. Biophys. Acta Bioenergy 1767 (9), 1073–1101.

Bernhard, G., Geipel, G., Reich, T., Brendler, V., Amayri, S., Nitsche, H., 2001. Uranyl(VI) carbonate complex formation: validation of the Ca2UO2(CO3)3(aq.) species. Radiochim. Acta 89, 511–518.

Bonhoure, I., Meca, S., Marti, V., De Pablo, J., Cortina, J.L., 2007. A new time-resolved laser-induced fluorescence spectrometry (TRLFS) data acquisition procedure applied to the uranyl-phosphate system. Radiochim. Acta 95, 165–172.

Brachmann, A., Geipel, G., Bernhard, G., Nitsche, H., 2002. Study of uranyl(VI) malonate complexation by time resolved laser-induced fluorescence spectroscopy (TRLFS). Radiochim. Acta 90, 147–153.

Brendler, V., Geipel, G., Bernhard, G., Nitsche, H., 1996. Complexation in the system $UO2^{2+}/PO_4^{3-}/OH^-$ (aq): potentiometric and spectroscopic investigations at very low ionic strengths. Radiochim. Acta 74, 75–80.

Brookshaw, D., Pattrick, R., Lloyd, J., Vaughan, D., 2012. Microbial effects on mineral–radionuclide interactions and radionuclide solid-phase capture processes. Mineral. Mag. 76, 777–806.

Burns, P.C., 1999. The crystal chemistry of uranium. Rev. Mineral. Geochem. 38, 23–90.

Cardenas, E., Wu, W.-M., Leigh, M.B., Carley, J., Carroll, S., Gentry, T., et al., 2008. Microbial communities in contaminated sediments, associated with bioremediation of uranium to submicromolar levels. Appl. Environ. Microbiol. 74, 3718–3729.

Cheung, K., Gu, J.-D., 2007. Mechanism of hexavalent chromium detoxification by microorganisms and bioremediation application potential: a review. Int. Biodeterior. Biodegrad. 59, 8–15.

Cho, D.H., Chu, K.H., Kim, E.Y., 2011. Lead uptake and potentiometric titration studies with live and dried cells of Rhodotorula glutinis. World J. Microbiol. Biotechnol. 27, 1911–1917.

de Silóniz, M.-I., Payo, E.-M., Callejo, M.-A., Marquina, D., Peinado, J.M., 2002. Environmental adaptation factors of two yeasts isolated from the leachate of a uranium mineral heap. FEMS (Fed. Eur. Microbiol. Soc.) Microbiol. Lett. 210, 233–237.

Dhal, P.K., Sar, P., 2014. Microbial communities in uranium mine tailings and mine water sediment from Jaduguda U mine, India: a culture independent analysis. J. Environ. Sci. Health, Part A 49, 694–709.

Fomina, M., Charnock, J.M., Hillier, S., Alvarez, R., Livens, F., Gadd, G.M., 2008. Role of fungi in the biogeochemical fate of depleted uranium. Curr. Biol. 18, R375–R377.

Galichet, A., Sockalingum, G.D., Belarbi, A., Manfait, M., 2001. FTIR spectroscopic analysis of Saccharomyces cerevisiae cell walls: study of an anomalous strain exhibiting a pink-colored cell phenotype. FEMS (Fed. Eur. Microbiol. Soc.) Microbiol. Lett. 197 (2), 179–186.

Geipel, G., 2006. Laser-induced fluorescence spectroscopy. In: Vij, D.R. (Ed.), Handbook of Applied Solid State Spectroscopy. Springer, New York, pp. 577–593.

Geipel, G., Bernhard, G., Rutsch, M., Brendler, V., Nitsche, H., 2000. Spectroscopic properties of uranium (VI) minerals studied by time-resolved laser-induced fluorescence spectroscopy (TRLFS). Radiochim. Acta 88, 757–762.

Gerber, U., Zirnstein, I., Krawczyk-Bärsch, E., Lünsdorf, H., Arnold, T., Merroun, M., 2016. Combined use of flow cytometry and microscopy to study the interactions between the gram-negative betaproteobacterium Acidovorax facilis and uranium (VI). J. Hazard Mater. 317, 127–134.

Gustafsson, J.P., Dässman, E., Bäckström, M., 2009. Towards a consistent geochemical model for prediction of uranium (VI) removal from groundwater by ferrihydrite. Appl. Geochem. 24, 454–462.

Hudson, E., Allen, P., Terminello, L., Denecke, M., Reich, T., 1996. Polarized x-ray-absorption spectroscopy of the uranyl ion: comparison of experiment and theory. Phys. Rev. B 54, 156.

Hufton, J., Harding, J.H., Romero-González, M.E., 2016. The role of extracellular DNA in uranium precipitation and biomineralisation. Phys. Chem. Chem. Phys. 18 (42), 29101–29112.

IAEA, 2003. Technical Basis for the Geological Disposal of Radioactive Wastes. Technical Report Series.

Imlay, J.A., 2003. Pathways of oxidative damage. Annu. Rev. Microbiol. 57, 395–418.

Jroundi, F., Merroun, M.L., Arias, J.M., Rossberg, A., Selenska-Pobell, S., González-Muñoz, M.T., 2007. Spectroscopic and microscopic characterization of uranium biomineralization in Myxococcus xanthus. Geomicrobiol. J. 24, 441–449.

Kato, Y., Meinrath, G., Kimura, T., Yoshida, Z., 1994. A study of U(VI) hydrolysis and

carbonate complexation by time-resolved laser-induced fluorescence spectroscopy (TRLFS). Radiochim. Acta 64, 107–111.
Koban, A., Geipel, G., Rossberg, A., Bernhard, G., 2004. Uranium (VI) complexes with sugar phosphates in aqueous solution. Radiochim. Acta 92, 903–908.
Koning, A.J., Lum, P.Y., Williams, J.M., Wright, R., 1993. DiOC6 staining reveals organelle structure and dynamics in living yeast cells. Cytoskeleton 25, 111–128.
Kulkarni, S., Ballal, A., Apte, S.K., 2013. Bioprecipitation of uranium from alkaline waste solutions using recombinant Deinococcus radiodurans. J. Hazard Mater. 262, 853–861.
Kumar, R., Nongkhlaw, M., Acharya, C., Joshi, S.R., 2013. Uranium (U)-tolerant bacterial diversity from U ore deposit of domiasiat in North-East India and its prospective utilisation in bioremediation. Microb. Environ. 28, 33–41.
Li, Z., Yuan, H., Hu, X., 2008. Cadmium-resistance in growing Rhodotorula sp. Y11. Bioresour. Technol. 99, 1339–1344.
Liang, X., Hillier, S., Pendlowski, H., Gray, N., Ceci, A., Gadd, G.M., 2015. Uranium phosphate biomineralization by fungi. Environ. Microbiol. 17, 2064–2075.
Liang, X., Csetenyi, L., Gadd, G.M., 2016. Uranium bioprecipitation mediated by yeasts utilizing organic phosphorus substrates. Appl. Microbiol. Biotechnol. 100, 5141–5151.
Lloyd, J.R., Renshaw, J.C., 2005. Microbial transformations of radionuclides: fundamental mechanisms and biogeochemical implications. Met. Ions Biol. Syst. 44, 205–240.
Lopez-Fernandez, M., Fernandez-Sanfrancisco, O., Moreno-Garcia, A., Martin-Sanchez, I., Sanchez-Castro, I., Merroun, M.L., 2014. Microbial communities in bentonite formations and their interactions with uranium. Appl. Geochem. 49, 77–86.
Lopez-Fernandez, M., Cherkouk, A., Vilchez-Vargas, R., Jauregui, R., Pieper, D., Boon, N., et al., 2015. Bacterial diversity in bentonites, engineered barrier for deep geological disposal of radioactive wastes. Microb. Ecol. 70, 922–935.
Lu, X., Zhou, X-j, Wang, T-s, 2013. Mechanism of uranium (VI) uptake by Saccharomyces cerevisiae under environmentally relevant conditions: batch, HRTEM, and FTIR studies. J. Hazard Mater. 262, 297–303.
Lütke, L., Moll, H., Bachvarova, V., Selenska-Pobell, S., Bernhard, G., 2013. The U (VI) speciation influenced by a novel Paenibacillus isolate from Mont Terri Opalinus clay. Dalton Trans. 42, 6979–6988.
Makarov, E., Ivanov, V., 1960. The crystalline structure of $Ca(UO_2)^2$ (PO_4) 2.6 H_2O meta-otenite. Dokl. Akad. Nauk SSSR 132, 673–676.
Martinez, R.J., Wu, C.H., Beazley, M.J., Andersen, G.L., Conrad, M.E., Hazen, T.C., et al., 2014. Microbial community responses to organophosphate substrate additions in contaminated subsurface sediments. PLoS One 9, e100383.
Masurat, P., Eriksson, S., Pedersen, K., 2010. Microbial sulphide production in compacted Wyoming bentonite MX-80 under in situ conditions relevant to a repository for high-level radioactive waste. Appl. Clay Sci. 47 (1–2), 58–64.
Merroun, M., Hennig, C., Rossberg, A., Reich, T., Selenska-Pobell, S., 2003a. Characterization of U (VI)-Acidithiobacillus ferrooxidans complexes using EXAFS, transmission electron microscopy, and energy-dispersive X-ray analysis. Radiochim. Acta 91, 583–592.
Merroun, M.L., Geipel, G., Nicolai, R., Heise, K.-H., Selenska-Pobell, S., 2003b. Complexation of uranium (VI) by three eco-types of Acidithiobacillus ferrooxidans studied using time-resolved laser-induced fluorescence spectroscopy and infrared spectroscopy. Biometals 16, 331–339.
Merroun, M.L., Raff, J., Rossberg, A., Hennig, C., Reich, T., Selenska-Pobell, S., 2005. Complexation of uranium by cells and S-layer sheets of Bacillus sphaericus JG-A12. Appl. Environ. Microbiol. 71, 5532–5543.
Merroun, M.L., Nedelkova, M., Ojeda, J.J., Reitz, T., Fernandez, M.L., Arias, J.M., et al., 2011. Bio-precipitation of uranium by two bacterial isolates recovered from extreme environments as estimated by potentiometric titration, TEM and X-ray absorption spectroscopic analyses. J. Hazard Mater. 197, 1–10.
Moll, H., Lütke, L., Cherkouk, A., 2015. Bacterial Diversity in Clay and Actinide Interactions with Bacterial Isolates in Relation to Nuclear Waste Disposal. Radionuclides in the Environment. Springer, pp. 209–229.
Morcillo, F., Gonzalez-Munoz, M.T., Reitz, T., Romero-Gonzalez, M.E., Arias, J.M., Merroun, M.L., 2014. Biosorption and biomineralization of U(VI) by the marine bacterium Idiomarina loihiensis MAH1: effect of background electrolyte and pH. PLoS One 9, e91305.
Moulin, C., Laszak, I., Moulin, V., Tondre, C., 1998. Time-resolved laser-induced fluorescence as a unique tool for low-level uranium speciation. Appl. Spectrosc. 52, 528–535.
Nedelkova, M., Merroun, M.L., Rossberg, A., Hennig, C., Selenska-Pobell, S., 2007. Microbacterium isolates from the vicinity of a radioactive waste depository and their interactions with uranium. FEMS (Fed. Eur. Microbiol. Soc.) Microbiol. Ecol. 59, 694–705.
North, N.N., Dollhopf, S.L., Petrie, L., Istok, J.D., Balkwill, D.L., Kostka, J.E., 2004. Change in bacterial community structure during in situ biostimulation of subsurface sediment cocontaminated with uranium and nitrate. Appl. Environ. Microbiol. 70, 4911–4920.
Olivelli, M.S., Schampera, B., Woche, S.K., Torres Sanchez, R.M., Curutchet, G.A., 2017. Importance of the hydration degree in the use of clay–Fungal biocomposites as adsorbents for uranium uptake. Ind. Eng. Chem. Res. 56, 2824–2833.
Pedersen, K., 2002. Microbial processes in the disposal of high level radioactive waste 500 m underground in Fennoscandian shield rocks. Radioact. Environ. 2, 279–311.
Pedersen, K., 2010. Analysis of copper corrosion in compacted bentonite clay as a function of clay density and growth conditions for sulfate-reducing bacteria. J. Appl. Microbiol. 108 (3), 1094–1104.
Pentráková, L., Su, K., Pentrák, M., Stucki, J.W., 2013. A review of microbial redox interactions with structural Fe in clay minerals. Clay Miner. 48, 543–560.
Poulain, S., Sergeant, C., Simonoff, M., Le Marrec, C., Altmann, S., 2008. Microbial investigations in Opalinus clay, an argillaceous formation under evaluation as a potential host rock for a radioactive waste repository. Geomicrobiol. J. 25, 240–249.
Prévéral, S., Gayet, L., Moldes, C., Hoffmann, J., Mounicou, S., Gruet, A., et al., 2009. A common highly conserved cadmium detoxification mechanism from bacteria to humans heavy metal tolerance conferred by the ATP-binding cassette (ABC) transporter SpHMT1 requires glutathione but not metal-chelating phytochelatin peptides. J. Biol. Chem. 284, 4936–4943.
Ravel, B., Newville, M. Athena, 2005. ARTEMIS, HEPHAESTUS: data analysis for X-ray absorption spectroscopy using IFEFFIT. J. Synchrotron Radiat. 12, 537–541.
Reitz, T., Rossberg, A., Barkleit, A., Steudtner, R., Selenska-Pobell, S., Merroun, M.L., 2015. Spectroscopic study on uranyl carboxylate complexes formed at the surface layer of Sulfolobus acidocaldarius. Dalton Trans. 44 (6), 2684–2692.
Romero-González, M., Nwaobi, B.C., Hufton, J.M., Gilmour, D.J., 2016. Ex-situ bioremediation of U (VI) from contaminated mine water using Acidithiobacillus ferrooxidans strains. Front. Environ. Sci. 4, 39.
Sánchez-Castro, I., Amador-García, A., Moreno-Romero, C., López-Fernández, M., Phrommavanh, V., Nos, J., et al., 2017. Screening of bacterial strains isolated from uranium mill tailings porewaters for bioremediation purposes. J. Environ. Radioact. 166, 130–141.
Sitaud, B., Solari, P.L., Schlutig, S., Llorens, I., Hermange, H., 2012. Characterization of radioactive materials using the MARS beamline at the synchrotron SOLEIL. J. Nucl. Mater. 425, 238–243.
SKB, A., 1999. Deep Repository for Spent Nuclear Fuel. SR-97–Post-closure Safety. SKB technical report 99–06.
Solari, P.L., Schlutig, S., Hermange, H., Sitaud, B.M.A.R.S., 2009. A new beamline for radioactive matter studies at SOLEIL. J. Phys. Conf. 190, 012042. IOP Publishing.
Stroes-Gascoyne, S., Sergeant, C., Schippers, A., Hamon, C.J., Nèble, S., Vesvres, M.H., et al., 2011. Biogeochemical processes in a clay formation in situ experiment: part D – Microbial analyses – synthesis of results. Appl. Geochem. 26, 980–989.
Villegas, L.B., Amoroso, M.J., de Figueroa, L.I., 2009. Responses of Candida fukuyamaensis RCL-3 and *Rhodotorula mucilaginosa* RCL-11 to copper stress. J. Basic Microbiol. 49, 395–403.
Wang, T., Zheng, X., Wang, X., Lu, X., Shen, Y., 2017. Different biosorption mechanisms of Uranium (VI) by live and heat-killed Saccharomyces cerevisiae under environmentally relevant conditions. J. Environ. Radioact. 167, 92–99.
Yurkov, A., 2017. Temporal and Geographic Patterns in Yeast Distribution. Yeasts in Natural Ecosystems: Ecology. Springer, pp. 101–130.
Zheng, X-y, Wang, X-y, Shen, Y-h, Lu, X., Wang, T-s, 2017. Biosorption and biomineralization of uranium (VI) by *Saccharomyces cerevisiae*. Crystal formation of chernikovite. Chemosphere 175, 161–169.